Arms races between selfish genetic elements and their host defence

Bitao Qiu[1 *], Daniel Elsner[1], Judith Korb[1, 2 *]

[1]Evolutionary Biology & Ecology, University of Freiburg, Germany

[2]Research Institute for the Environment and Livelihoods, Charles Darwin University, Casuarina Campus, NT0909 Darwin, Australia

[*] Email: bitao.qiu.88@gmail.com; judith.korb@biologie.uni-freiburg.de

Abstract

Arms races between parasites and hosts are key drivers of evolution. Selfishly replicating transposable elements (TEs) are thought to follow similar dynamics, but strong evidence is missing. We tested this in termites, social insects in which TEs have been linked to ageing. Sequencing genomes and profiling DNA methylation across the termite phylogeny revealed corresponding phylogenetic signals in TEs and TE methylation, indicative of selection. TE methylation reduces TE success, as both TE abundance and spreading efficiency decrease with increasing methylation. TEs also become less harmful with TE age: evolutionarily older TEs spread less, insert less into exons, and erode into short remnants. Correspondingly, defence through methylation is strongest against young TEs. Yet, as in typical host–parasite arms races, some TEs persist, implying resistance or recurrent invasions. Our results reveal arms races between TEs and DNA methylation, positioning TEs as drivers of genome evolution similar to symbionts in organismic evolution.

Introduction

Conflict can lead to antagonistic evolutionary arms races. When organisms continuously reduce their partners' fitness, they impose selection for defence mechanisms that can result in adaptations and counter-adaptations between co-evolving partners [1]. This is best known for prey/predator and host/parasite interactions. One of the best-studied examples is bats and moths. Bats use echolocation for moth-prey detection and moths evolved the ability to detect bat calls or confuse bats with click calls to evade capture [2,3]. We predict similar arms races at the organism level for genetic elements that behave selfishly, for instance, by replicating independently within a genome, which harms host fitness [4–6]. Yet, evidence for full-cycle evolutionary arms races is scarce, especially for the most abundant selfish genetic elements, transposable elements (TEs) [6,7].

TEs, often called 'jumping genes', can either (i) make a copy of themselves via an RNA intermediate that inserts at a new genomic position ('copy and paste' mechanism; retrotransposons, class I elements) or (ii) change their position within the host genome by excising themselves from one location and inserting into another ('cut' and 'paste' mechanism; DNA Transposons, class II elements)[8]. Furthermore, TEs have been classified into superfamilies and families based on sequence similarity [9]. Although TEs can sometimes provide genetic material for evolutionary innovation [10–13], their activity is commonly costly to the individual bearing them ('the host'). TEs can compromise genome functioning when jumping into genes or regulatory regions or cause costs through ectopic recombination [14–16]. Hence, TEs are commonly regarded as genomic parasites [5,6,17]. As expected for harming parasites, counter-mechanisms have evolved that protect the host against TEs by silencing TEs transcriptionally or post-transcriptionally [6,18–21]. The most important mechanisms are the piwi-interacting RNA (piRNA) pathway, which silences active TEs [22], and chromatin marks and DNA methylation, two conserved epigenetic mechanisms that repress TEs [6,23–27].

Although being a controversial topic [28], in many organisms somatic TE activity has been associated with ageing and age-related diseases, including termites [29–32]. Termites are social insects with genomes are typically composed of about 50% TEs [33,34]. Regardless of caste, senescent (old-aged) termite individuals are characterized by high TE activity that present a large potential threat. However, the long-lived queens and kings are better protected against TE activity than the short-lived workers[31,35]. This combination of high TE content and TE-associated caste-specific ageing makes termites a compelling system for studying the co-evolution between TEs and their hosts. This differs compared to social Hymenoptera like ants and bees, which harbour much fewer TEs in their genomes [36] . In addition, DNA methylation, which can constitutively silence TEs [6,26], is especially prevalent in termites in contrast to many other insects [34,37,38].

We test for evolutionary arms races between TEs and TE defence via DNA methylation in termites. We employ long-read sequencing, which overcomes biases from bisulfide short-read sequencing in profiling DNA methylation in repetitive regions like TEs [39]. [40,41]. We simultaneously sequence the genomes and measured DNA methylation levels from the same individuals of seven termite species across the termite phylogeny, along with six replicate

population samples of a focal species. By analysing the co-evolution pattern of TEs and TE DNA methylation in termites, we trace the evolutionary history of TEs and TE defence. We show that the harm of TEs to the host generally declines with TE age, while host defence through DNA methylation is strongest against young TEs. Our results reveal strong evidence for evolutionary arms races between TE and TE defence in termites.

Results

TEs and TE methylation patterns have strong evolutionary signals in termites

We used PacBio HiFi long-read systems to sequence high-molecular-weight DNA extracted from eight single individual samples of seven termite species that cover the full spectrum of termite social complexity. These species comprised *Mastotermes darwiniensis*, *Zootermopsis nevadensis*, *Cryptotermes secundus*, *Reticulitermes grassei*, *Trinervitermes geminatus*, *Macrotermes bellicosus* and *Odontotermes* sp.2 (**Fig. 1a**). For *M. bellicosus*, we sequenced both a queen and a soldier sample as species replication and to compare a potential caste effect on TE abundance and DNA methylation (see **Supplementary Note 1**). For each individual, we generated 17 to 40 Gb HiFi reads, with mean read length from 5,028 to 16,689 bp and estimated sequencing depth from 16 to 66x (**Supplementary Table 1**). We assembled our termite HiFi reads and obtained eight genome assemblies with sizes ranging from 576 Mb in *Z. nevadensis* to 1.4 Gb in *Odontotermes* sp.2 (**Fig. 1a**) (**Method**). Our genome assemblies had a genome completeness (coverage of the total BUSCO gene content) between 98.2% and 100% (**Fig. 1a**) (for further genome quality data, see also **Supplementary Table 1**), achieving high quality genome assemblies from single individuals.

To examine the distribution of TEs across the termite phylogeny, we built a non-redundant repeat library and annotated the repeat content (including TEs) in termites, including our eight termite genome assemblies and the published genome assembly of their sister taxon, *Cryptocercus punctulatus* woodroach [42]. Repeat content in the termite genomes ranged from 40.5% in *Z. nevadensis* to 61.3% in *M. darwiniensis* (**Fig. 1a**). Termite genome size correlated significantly with both the total size and the proportion of repetitive content (Pearson's $r = 0.99$ and 0.94, respectively; both $p < 0.001$) (**Supplementary Fig. 1**). This result supports the hypothesis that genome size variation in termites is driven by TE expansion and contraction [33], as in many other organisms [43,44].

Focusing on TE superfamilies, principal component analysis (PCA) showed that TE abundance (i.e., the copy numbers of different TE superfamilies in the genome; a measure of the replication success of TEs, comprising cumulatively active and non-active TEs) largely reflects termite phylogeny [45,46] (**Fig. 1b**). Principle component (PC) 1 separated the Geoisoptera (Termitidae and *R. grassei*) from the other termites, while PC2 separated Z. *nevadensis* from *C. secundus* and *M. darwiniensis*. We found a similar pattern with a clustering analysis (**Fig. 1c**). Among the top TE superfamilies that contribute to the two PCs, many had lineage/species specific distributions (**Supplementary Table 2**). For example, Mutator-like elements (MULE) and Maverick, two DNA transposon superfamilies, were only highly abundant in the Geoisoptera (**Supplementary Table 2**). By contrast, hAT DNA transposons and Alu short interspersed

nuclear elements (SINE) were restricted to *Z. nevadensis* (**Fig. 1c**) (**Supplementary Table 2**). This phylogenetic TE signal indicates lineage/species-specific TE evolution. This result contradicts the evolutionary model that TE evolution is largely driven by random drift effects [47] but it is in line with an evolutionary arms race scenario.

To test whether we can detect a corresponding TE defence signal, we quantified TE DNA methylation. To this end, we used the kinetic information from the PacBio HiFi reads to generate the methylation (5mC) probabilities for CpG sites in our termite genome assemblies (**Method** and see **Supplementary Note 2** for the validation of CpG methylation quantification). The genome-wide percentage of methylated CpG sites was not associated with termite phylogeny (**Fig. 1a**). However, CpG methylation levels (i.e. the percentages of methylated CpGs normalised by the whole genome background; hereafter TE methylation for simplicity) of TE superfamilies reflected the phylogeny of termites, showing a similar pattern as TE abundance. In a PCA, PC1 separated the Geoisoptera from *C. secundus* and PC2 separated Geoisoptera from *M. darwiniensis* and *Z. nevadensis* (**Fig. 1d**). Clustering analysis revealed a similar pattern with genomes from Geoisoptera clustering together in the dendrogram (**Fig. 1e**). In addition, the dendrogram based on TE methylation was largely consistent with that based on TE abundance (permutation test: $p < 0.01$) (**Supplementary Fig. 2**), as predicted by the evolutionary arms race hypothesis. These results show lineage/species-specific evolution of TE methylation but not of methylation in general, indicating that TE methylation is heritable, under natural selection and associated with TE abundance.

To gain further insights into potential drivers of these phylogenetic TE and TE methylation signals, we zoomed into individual TE superfamilies. Some TE superfamilies had consistent methylation patterns across all termite species (**Supplementary Table 3**). For example, LINE-2 and PiggyBac had high methylation levels across all genomes, while LINE-1 TEs were hypo-methylated (**Supplementary Table 3**). By contrast, other TE superfamilies revealed lineage/species-specific methylation patterns that were positively or negatively associated with their abundance in some parts of the phylogeny. For example, Pao LTR retrotransposons showed high abundance and high methylation levels in the Macrotermitinae, but low abundance and low methylation levels in *Z. nevadensis* and *M. darwiniensis*. In contrast, MULE and Maverick elements, which are both abundant in Geoisoptera, displayed low methylation levels in all species except *Z. nevadensis* and/or *M. darwiniensis* (**Fig. 1e**). This lineage/species-specific pattern can be explained by the evolutionary invasion history of the TE families (see **Supplementary Note 3**). Because methylation levels vary widely among TE families within each superfamily (**Supplementary Fig. 3**), finer-scale analyses at the TE family level are required to test for potential arms race dynamics.

TE abundance indicates TE and TE methylation arms race dynamics in termites

To study the arms races at the TE family level, we estimated the evolutionary age of TE families (hereafter, TE age) based on their lineage-specificity across the termite phylogeny (**Method**). We focused on *M. bellicosus* because our genome samples included closely related species (**Fig. 1a**), which allow us to identify species/lineage-specific TE families. Among the 2672 TE families in *M. bellicosus*, at least 31% (833 families) can be traced back more than 120 Ma to

153 the last common ancestor of *R. grassei* and *C. secundus* (Icoisoptera) (hereafter, ancient TE
154 families), while only 4% (102 families) were *M. bellicosus* specific (hereafter, young TEs) (**Fig.**
155 **2a**). The average TE sequence length significantly decreased with TE age (Spearman's r = -
156 0.16; p < 1e-5) (**Fig. 2b)**. TE length was nearly five times longer for young, *M. bellicosus*-
157 specific TE families than for ancient TE families (1535 bp vs. 259 bp). This indicates that
158 ancient TEs eroded or lost parts of their sequence, which could make them non-functional over
159 time.
160
161 If there are evolutionary arms races between TEs and TE methylation, we predict young,
162 species-specific TEs to be hypermethylated while ancient TE families are under-methylated.
163 This is because young, newly invaded TEs are more active and harmful to the host [17,48]. By
164 contrast, ancient TE families could be non-active due to erosion (**Fig. 2b**) or might even have
165 been evolutionary co-opted and perform host functions [13,49]. To test this, we examined the effect
166 of TE age on TE family methylation level in the *M. bellicosus* genome. Supporting an
167 evolutionary arms race scenario, both variables negatively correlated (Spearman's r = -0.19; p
168 < 1e-5) (**Fig. 2c**). Particularly, methylation levels of young *M. bellicosus*-specific TEs were
169 significantly higher than the genomic background (mean methylation level = 0.83, Student's t-
170 test: n = 101, p < 1e-5), while those of ancient TE families were significantly lower (mean
171 methylation level = -0.20; Student's t-test: n = 825; p < 1e-5) (see **Supplementary Fig. 4** for a
172 similar pattern in other termite species).
173
174 We also stratified TE families into recently expanded and more diverged families based on their
175 mean within-family sequence divergence, quantified by Kimura's distance (KD), an indicator
176 of the time since TE invasion/expansion in a species [36,50,51] (**Method**). Recently expanded TE
177 families generally contain highly similar TE copies with low mean KD values, whereas more-
178 diverged families, which are likely non-active, show greater sequence divergence due to the
179 accumulation of mutations, resulting in high mean KD values. Interestingly, while TE
180 methylation levels generally declined with TE age, more-diverged TE families (KD > 20) had
181 significantly higher methylation levels than recently expanded TE families (KD < 20) across
182 all TE age groups, except for ancient TE families that are likely eroded **(Supplementary Fig.**
183 **5** and **6)**. This result is consistent with the expectation that DNA methylation suppresses TE
184 proliferation and that methylation in ancient non-active families - which no longer pose a threat
185 to the host - is no longer maintained by natural selection.
186
187 Furthermore, if TE methylation functions as a means to silence TEs, TE abundance should
188 negatively correlate with TE methylation. As expected, TE abundance declined significantly
189 with TE methylation (Spearman's r = -0.25; p < 1e-5) (**Fig. 2d**). This applied also after
190 controlling for TE age, with a significant interaction between TE methylation and TE age
191 (ANCOVA; both $p_{TE\ methylation}$ and $p_{TE\ age}$ < 1e-5 and $p_{TE\ methylation\ x\ TE\ age}$ = 0.02), showing that
192 the TE methylation effect is most pronounced in younger TEs (**Supplementary Fig. 7**). We
193 also found similar negative correlations between TE methylation and TE abundance in other
194 termite genomes, stressing the generality of the results (**Supplementary Fig. 8**).
195
196 ***TE activity reveals TE and TE methylation arms race dynamics in M. bellicosus***

To measure the impact of TEs in the genome, we determined the number of TE-associated structure variants (SVs). TE-associated SVs indicate potential harm to the host because SVs are measures of mutation. In addition, as SVs are quantified within a population of a species, they also hint at currently active TEs (see also **Supplementary Note 4**) and their numbers correlate with the TEs replication success, a measure of TE fitness. To this end, we sequenced individual genomes from six *M. bellicosus* colonies to identify SVs and infer TE activities (**Method**). We found 267,001 SVs among the *M. bellicosus* samples and, by annotating the SVs with our termite repeat library, identified 172,157 (64%) TE-associated SVs (**Method**).

We found a striking observed abundance bias for the locations of TE-associated SVs that implies selection against harmful exonic insertions. Among the TE-associated SVs, only 1.5% (2249) were located in exons, while the rest were located in introns (55.2%) or intergenic (43.3%) regions. This observed abundance bias persisted after controlling for the sequence length of introns and exons, with TE-associated SVs 2.8 times less likely to be observed in exonic than in intronic regions (two sample Z-test of proportions: $p < 1e\text{-}5$). Furthermore, comparing the exonic insertion ratio (i.e., the number of exonic to total insertions) across TE families revealed a significant decline with increasing TE family abundance (Spearman's r = -0.28; $p < 1e\text{-}5$) (**Supplementary Fig. 9**), indicating that exonic insertions are more strongly selected against and hence less successful. In addition, the exonic insertion ratio declined with TE family age (Spearman's r = -0.1; $p < 1e\text{-}5$) (**Fig. 3a**). In particular, the exonic insertion ratio for ancient TE families was almost four times lower than that for young, *M. bellicosus*-specific TE families (0.026 vs. 0.106; Student's *t*-test: $p < 1e\text{-}5$), suggesting that ancient TEs are less harmful to the host.

On the opposite side, TE family success was associated with a young age. The proportion of highly active TE families (copy number of TE-associated SVs > 3) was significantly higher in young, *M. bellicosus*-specific TE families than ancient TE families (71 out of 103 *vs.* 493 out of 845 TE families; 69.0% *vs.* 58.3%; Fisher's exact test: $p < 5e\text{-}5$), as expected when young TEs are more likely to mobilize [52] . In addition, TE family spreading efficiency, measured as the ratio between TE-associated SVs and TE abundance (a measure of TE success) (**Method**), was negatively correlated with TE age (Spearman's r = -0.38; $p < 1e\text{-}5$) (**Fig. 3b**). This holds for DNA transposons or retrotransposons (**Supplementary Fig. 10**). Young, *M. bellicosus*-specific TE families were 3.2 times more successful in spreading than ancient TE families. Thus, young TE families are more likely to be active and are more efficient in spreading than older ones.

When TE DNA methylation functions as a defence mechanism that can suppress TEs, we predict a negative correlation between TE methylation and the spreading efficiency of TE families. As expected, over all TE age groups, TE families with high methylation had a lower TE spreading efficiency (Spearman's r = -0.14; $p < 5e\text{-}5$). Similar to the pattern with TE abundance (**Fig. 2d**), the effect of TE methylation on TE spreading efficiency applied even after controlling for the effect of TE age with a significant interaction effect between TE methylation and TE age (ANCOVA: both $p_{TE\ methylation}$ and $p_{TE\ age} < 1e\text{-}5$ and $p_{TE\ methylation\ X\ TE\ age} < 1e\text{-}3$). The correlation coefficient between TE spreading efficiency and TE methylation was positively

241 associated with TE age (Spearman's r = 0.7; p = 0.23), increasing from -0.46 in young, *M.*
242 *bellicosus*-specific TE families to -0.04 in ancient TE families (Spearman correlation tests: $p <$
243 1e-5 and p = 0.23, respectively) (**Fig. 3d**). This implies that the selection pressure on the host
244 to defend itself against TEs declines with TE age, in line with ancient TEs being less harmful,
245 as indicated by their lower exonic abundance, reduced spreading efficiency, and sequence
246 erosion.
247
248 ***Top active TE families can have ancient origins***

249 To analyse the origin of the top active TE families, we identified the top 100 TE families with
250 the highest number of TE-associated SVs in the *M. bellicosus* genome. We found that BovB
251 (LINE) (n_{family} = 26) and Tc1/mariner (DNA transposon) (n_{family} = 13) were among the top three
252 active TE superfamilies (**Fig. 4a**), consistent with previous findings that BovB and Mariner are
253 highly active in *M. bellicosus* [31]. In line with their high activity, their mean methylation levels
254 were lower than that of the genomic background (Student's t-tests: p_{BovB} = 0.01, $p_{Tc1/mariner}$ =
255 0.05) (**Fig. 4b**). Interestingly, thirteen (33%) of these 39 top-active BovB and Tc1/mariner TE
256 families were ancient TEs (**Fig. 4a**), suggesting top-active TEs can have ancient origins.
257
258 To trace the evolutionary histories of these ancient TE families, we further inspected the
259 distribution of their within-family sequence divergence (KD values among TE copies within
260 the same family). While mean KD values reflect the overall divergence of a TE family, the
261 distribution of KD values within a family reveals the composition of its members. Consistent
262 with their high activities in *M. bellicosus*, KD frequency distributions for the majority (9 out of
263 13) of these TE families had a mode with KD values lower than 10, indicative of recently
264 expanded TE copies, and these modes were largely absent in the non-Termitidae genomes (**Fig.
265 4c**). This suggests that they were recent expansions/invasions in *M. bellicosus*, despite being
266 ancient TEs. Seven of these nine TE families also had an additional second mode in *M.
267 bellicosus* and a single mode in many other termite species, all of which had KD values higher
268 than 20 (**Fig. 4c** and **Supplementary Fig. 11**), reflecting high sequence divergence probably
269 due to many TE remnants (decayed, non-active TE copies) and ancient invasions. Our results
270 imply that these seven TE families have copies of ancient origin and copies recently expanded
271 in *M. bellicosus*.
272
273 ***TE defence genes are under strong selection in the termite genomes***

274 If TEs play a major role as parasites of termite genomes, we predict selection on TE defence
275 genes. These include genes involved in DNA methylation and retrotransposon silencing,
276 particularly those from the piRNA pathway that mediate DNA methylation to silence TEs [6,18,19].
277 Thus, we examined whether TE defence genes are under positive selection in our termite
278 genomes, using the woodroach as outgroup [53,54] (**Method**). Forty-nine TE defence genes were
279 present in both the woodroach and termites. Among these genes, 15 (31%) exhibited a signature
280 of positive selection in the termites, which was significantly higher than expected based on the
281 whole genome background (7%) (two-sided binomial test: $p <$ 1e-5). Ten (32%) out of the 31
282 piRNA pathway genes were under positive selection. For example, both aubergine (*Aub*) and
283 *qin*, which are differentially expressed between young and old *M. bellicosus* workers [31], were

under positive selection in the lineage leading to the Macrotermitinae. Several piRNA pathway genes have also been repeatedly selected in multiple termite lineages/species (**Supplementary Fig. 12**), indicating their important roles in the evolutionary arms races with TEs.

Discussion

Our results revealed evolutionary arms races between TEs and TE methylation in termites (**Fig. 5**). Such arms races typically involve: (i) Parasites that harm a host, (ii) host defences against the parasite, (iii) co-evolution of parasite virulence and host defence, and (iv) evolutionary outcomes ranging from parasites being permanently 'shut down' and becoming commensals or even mutualists, to recurrent arms races [1,14,55,56]. We found support for all of these components.

TEs as parasites. As former studies have also shown [33,34], TEs account for around 50% of termite genome (except *Z. nevadensis*) with genome size correlating with TE content (**Supplementary Fig. 1** and **Supplementary Note 5**). This reflects their accumulation over time and their huge importance for their host. Their harm has been shown in ageing studies that associate ageing and senescence with TE activity and the extraordinarily long lifespan of the queen and king with TE defensive mechanisms [31,57].

TE methylation as host defence against TEs. As predicted, when TE methylation suppresses TEs, our study showed that both TE abundance (i.e., active and formerly active TEs) and, more importantly, TE spreading efficiency (i.e., the success of currently active TEs) declined with increasing TE methylation in termites (**Fig. 2d** and **Fig. 3b)**. Thus, our study also supports the emerging evidence that DNA methylation, although less common in some insect orders [58–60], can play an important role in insects and their defence against TE [23,60]. Importantly, as TE spreading efficiency can be seen as a direct measure of TE fitness, our result demonstrates that TE methylation impedes TE success. Thus, TE methylation is a host defence mechanism that ultimately benefiting the host. Hence, our study establishes, for the first time, a direct link between DNA methylation and TE success.

Co-evolution of virulence and host defence. We found clear evolutionary age effects, indicative of co-evolution between TEs and termite defence via TE methylation (i.e. they reciprocally affect each other through processes of natural selection). On average, TE virulence (harm to the host) declined with the evolutionary age of TE families, and accordingly, selection on host defence weakened as well.

Evidence for a decline of TE virulence comes from the following three results. First, the spreading efficiency of TEs - and hence their potential harm - declined with TE age (**Fig. 3b**). Because TE methylation negatively affected spreading efficiency (**Fig. 3c**), the age-related decline in TE spreading efficiency is likely, at least in part, a consequence of host defence. Second, although some ancient TEs remain active, most are probably inactive remnants, as indicated by their substantially reduced sequence length (**Fig. 2b**), low spreading efficiency (**Fig. 3b**) and high sequence divergence (**Supplementary Fig. 5**). Third, exonic TE insertions, which are generally more harmful than insertions in other regions [61], were less common in

ancient than in younger TEs (**Fig. 3a**). This systematic difference in exonic insertion bias likely reflects natural selection: harmful TEs are purged over time, but because selection acts with a time lag, young TEs still retain more harmful insertions than ancient ones. The efficiency of this purging depends on the strength of selection, which in turn varies with TE virulence as well as factors such as population size and genetic drift [62,63].

In line with the reduced harm of TEs with evolutionary age, selection on host defence was more effective in silencing younger than ancient TEs. Associations between TE methylation and both TE abundance and TE spreading efficiency were stronger in young than in ancient TEs (**Supplementary Fig. 7** and **Fig. 3c**). This pattern reflects co-evolution between TE virulence and TE defence. As the virulence of older TEs declines, the selection pressure to silence ancient TEs weakens, while when young TEs invade, the pressure to silence them strengthens. Accordingly, many TE defence genes - especially from the piRNA pathway, which also mediates DNA methylation - were repeatedly under positive selection in termites (**Supplementary Fig. 12**).

Variable arms race outcomes. Yet, not all ancient TEs are inactivated and harmless to the host. Some of the most active TEs, such as BovB and Tc1/mariner elements linked to ageing and senescence in *M. bellicosus* [31], appear to have ancient origins, as indicated by their high KD values (**Fig. 4c**). These TEs might have escaped silencing through methylation, making them currently evolutionary 'winners' of the arms race. Similarly, in *D. melanogaster*, TEs have been shown to employ counter-defence strategies against host silencing, including "anti-silencing" mechanisms [64]. We observed that the same TE families can be highly abundant and active in phylogenetically distant termite species, yet absent in others (**Supplementary Table 2b**). Such patterns may reflect recent invasions via horizontal transfer [65,66] and could elicit strong selection in the host, as has been shown in *Drosophila* [48]. Finally, some TEs can be co-opted by host genomes, contributing to regulatory rewiring, immune responses, or development [67–70], and thus provide raw material for novel functions and adaptation [71,72].

These variable outcomes reflect a pattern typical for interspecific associations known as symbioses, where gradients ranging from parasitism via commensalism to mutualism exist, with TE virulence and the nature of association between TEs and the host changing over time [1,14]. While it remains to be tested whether TEs can be beneficial mutualists in termites, it has been hypothesized that TE-induced gene tandem duplications might have been co-opted for caste-specific gene expression [33]. We expect that, on average, ancient TEs are more likely to develop such beneficial functions compared to younger ones due to long-term co-evolution with the host. Viewing TEs as evolving symbionts reconciles empirical findings and debates over whether they are harmful parasites, neutral genetic elements, or drivers of beneficial innovation. Ultimately, they are symbionts with effects on their hosts that vary over time and context.

Methods

Individual termite samples for genome sequencing

For *Cryptotermes secundus*, *Mastotermes darwiniensis*, *Reticulitermes grassei* and *Zootermopsis nevadensis*, a queen (for *R. grassei*) or a worker (for other species) had been collected from lab colonies housed at the University of Freiburg. *C. secundus* had been collected at Channel Island, Australia, in 2019; *M. darwiniensis* colony in Darwin, Australia, in 2022, *R. grassei* on Île d'Oléron, France, in 2020 (donated by Franck Dedeine), *Z. nevadensis* in 2023 in California, the United States. These colonies had been kept in climate chambers in Freiburg, Germany, and the individual termites were freshly killed in 2023 to extract DNA.

For the other species, samples had been collected in the field and stored in 100% ethanol or RNAlater (QIAGEN, Cat no. 76106) at -20 °C until DNA extraction. A *Trinervitermes geminatus* worker in Lamto, Côte d'Ivoire, in 2021; a *Odontotermes* sp.2 queen in the Comoé National Park, Côte d'Ivoire, in 2019; a *Macrotermes bellicosus* queen and a minor soldier in the Comoé National Park, Côte d'Ivoire in 2017. Besides, four minor workers of *M. bellicosus* were collected from different colonies between 2018 and 2019 in the Comoé National Park, Côte d'Ivoire to detect structure variants (SVs) in *M. bellicosus.*

DNA extraction and sequencing

Because the body sizes of our sampled termite species differ by several orders of magnitude, to achieve individual genome sequencing, genomic DNA was extracted from heads (for *M. darwiniensis, Z. nevadensis* and *M. bellicosus* workers and soldier*),* dissected fat bodies (for *M. bellicosus* and *Odontotermes* sp.2 queens), or from gut-removed whole bodies (for the *R. grassei* queen and *T. geminatus* and *C. secundus* workers) (**Supplementary Table 1**). DNA extractions were carried out using the 2% cetyltrimethylammonium bromide (CTAB) protocol [73] with minor modifications (cut pipette tips to obtain high molecular weight DNA; digesting proteins with over-night proteinase K incubation to increase DNA yield). DNA sample quality was tested with a NanoDrop and DNA fragment sizes were by agarose gel electrophoresis.

Depending on the amount of extracted DNA, low DNA input or standard DNA input libraries (**Supplementary Table 1**) were constructed for single-molecule real-time (SMRT) sequencing. For the four *M. bellicosus* minor workers used for detecting SVs, ultra-low DNA input libraries were constructed because of the small amount of DNA. Long high-fidelity (HiFi) reads were generated with the Pacific Biosciences (PacBio) Sequel II or the PacBio Revio system.

Genome assembly

The genomes of the seven termite species were assembled with *Hifiasm* (v.0.19.5) [74] (with *--dual-scaf* for self-scaffolding and other default parameters for HiFi reads only genome assembly), a *de novo* assembler for PacBio HiFi reads. We noticed that the *T. geminatus* genome assembly had > 10% duplicated BUSCOs (Benchmarking Universal Single-Copy Orthologs) (v5.6.0 with insecta_odb10) significantly more than the other termite genome

408 assemblies. We reason that the higher BUSCO duplication rate may be caused by the lower
409 sequencing depth in *T. geminatus* because a lower sequencing depth can lead to false
410 duplications in diploid genomes with high genomic heterozygosity [75]. To remove false
411 duplications, we employed a second round of haplotig-duplication purging on the *T. geminatus*
412 genome assembly with *purge_dups* (v. 1.2.6) and with the *-e* option to only purge haplotypic
413 duplications at the ends of contigs [76]. All genome assemblies were screened to remove potential
414 contamination with Foreign Contamination Screening (FCS-GX) [77].

415

416 **Genome assembly evaluation**

417 The genome assemblies of the seven termite species were evaluated using BUSCO (v.5.6.0 with
418 insecta_odb10) [78] for gene content completeness, Merqury (v1.3) [79] for k-mer completeness
419 ($k = 21$) and assembly consensus quality value (QV), and GenomeScope 2.0 [80] for k-mer-based
420 ($k = 21$) haploid genome length, heterozygosity, and repeat length estimation. For *T. geminatus*,
421 both the pre- and post-deduplicated assemblies were assessed.

422

423 **Building a non-redundant termite repeat library**

424 To improve the completeness of TE discovery and ensure comparability across species, we
425 generated a non-redundant repeat library for termites. We first used RepeatModeler (v. 2.0.5)
426 [81] (default parameters and *-LTRStruct* for running LTR structural search pipeline) to build eight
427 de-novo repeat libraries from our seven termite genome assemblies (for *M. bellicosus*, we used
428 the queen genome assembly) and the in-house *Cryptocercus punctulatus* (woodroach) genome.
429 To reduce redundant TE families and to minimize false TEs due to high copy-number genes
430 (such as olfactory receptor coding genes), we curated the repeat libraries using MCHelper
431 (v1.6.6) [82] (default parameters and with *-b* option to filter out false TEs with BUSCO genes
432 q[insecta_odb10]). We then merged the filtered repeat libraries into one redundant multi-
433 species repeat library.

434

435 To reduce redundancy caused by orthologous TE families appearing multiple times in the
436 redundant repeat library (e.g. when a TE family originated in the last common ancestor of *M.*
437 *bellicosus* and *O.* sp2, resulting in two copies), we sorted the consensus sequences of TE
438 families by size into the following categories: <500 bp, 500 bp – 1kb, 1kb – 2kb, 2kb – 5kb,
439 5kb – 10kb, 10 kb – 20kb and > 20kb. Within each size category, we clustered TE families
440 based on sequence similarity (≥90%) using the *ClusterPartialMatchingSubs.pl* script from
441 RepeatModeler2, with the 90% cut-off chosen to balance sensitivity and specificity [83]. For each
442 TE family cluster, we retained the longest sequence as the representative sequence. Finally, we
443 obtained a non-redundant repeat library for termites by combining the representative sequences
444 of the TE family clusters and that of the unique TE families, which only occurred in one species.
445 TE sequences in the non-redundant repeat library were then classified with *RepeatModeler2*,
446 using the Repbase (RepeatMasker Edition v20181026) [84] and the Dfam (v.3.8) [85] TE databases.
447

448 **Repeat annotation in genome assemblies**

449 Using the classified non-redundant repeat library for termites, we annotated repeats in each
450 genome assembly with *RepeatMasker* (v. 4.1.7) [86] (default parameters and using rmblast for
451 searching sequences). To accurately quantify TE copy numbers, we applied One-code-to-find-
452 them-all [87] (default parameters) to link TE fragments likely derived from the same TE copies.
453 We then summarised the number of TE copies for each TE family in each genome assembly.
454 To minimize false TE identifications, only TE families with more than 3 copies were retained
455 for downstream analyses.
456
457 For superfamily-level analyses (e.g., PCA and dendrogram analyses), only classified TE
458 families were included, as unclassified TEs cannot be assigned to superfamilies. For other
459 analyses (e.g., TE age and the association between TE abundance and TE methylation at the
460 family level), including or excluding unclassified TE families yielded similar results. Because
461 unclassified TEs may contain false positives, they were excluded from our analyses.
462
463 **Exons and introns annotation**

464 Genomic regions of the seven termite species and the woodroach (*C. punctulatus*) were
465 annotated by combining the Braker3 (v3.0.8) [88] and the StringTie (v2.2.1) [89] pipelines. For each
466 species, the genome assembly was first soft-masked with RepeatMasker (see *Repeat annotation*
467 *in genome assemblies*). For *M. darwiniensis*, *R. grassei*, *O.* sp. 2, and *T. geminatus*, in-house
468 RNA-seq data (from another project) were used, following our in-house protocol for data
469 generation and quality control [90]. In-house or published RNAseq data [31,34,90,91] were then
470 mapped to the target genome with *Hisat2* (v. 2.2.1) [92] with the *--dta* option to report alignments
471 tailored for transcript assemblers.

472 The masked genome was then annotated with both StringTie, which used only RNAseq data,
473 and Braker3, which incorporated RNA-seq data, protein data (Arthropoda orthologs from
474 OrthoDB 11), and BUSCO data (insecta_odb10) [93]. The Braker and the StringTie annotations
475 were then merged and annotated with Transdecoder (v5.71) [94] (default parameters; BlastP
476 [UniRef90] and Pfam searches enabled to retain ORFs based on homology), which predicts
477 protein-coding genes and annotates exons, introns and untranslated regions.

478 Because the StringTie annotation can include transposons with coding regions, the merged
479 genome annotations were scanned using InterProScan (v5.68) [95] (default parameters) so that
480 genes with transposon-related domains (such as the transposase DDE domain) were removed
481 from the final annotations.

482 For *M. bellicosus*, the queen genome assembly was selected as the representative genome for
483 annotation, as it had higher quality than the soldier assembly, based on N50 and BUSCO
484 metrics (**Supplementary Table 1**).
485
486 **Estimation of the evolutionary age of TE families**

487 The ages of TE families were estimated based on their distribution across the termite phylogeny.
488 In principle, if a TE family occurs in a specific lineage or species but is absent in others, we

489 considered it to be lineage- or species-specific. To determine the presence or absence of TE
490 families, we used effective copy numbers (ECN), calculated as the total sequence length of all
491 TE copies in a family divided by its consensus sequence length. A TE family was considered
492 present if its ECN > 5.
493
494 We classified TE families' ages into the following age groups:
495
496 *M. bellicosus*-specific: Present in *M. bellicosus* (either in the queen or soldier genome) but
497 absent in other species. Since *M. darwiniensis* and *C. punctulatus* have been evolutionary
498 separated from other termite lineages for over 120 million years, any similar TEs found in both
499 *M. bellicosus* and either of the two species are likely due to re-introduction. Therefore, we
500 excluded *M. darwiniensis* and *C. punctulatus* from the TE age analysis in this and subsequent
501 sections.
502
503 *O. sp2*.-specific: Present in *O. sp2.* but absent in other species.
504
505 Macrotermitinae-specific: Present in *M. bellicosus* and *O. sp2.* but absent in other species.
506 Termitidae-specific: Present in Macrotermitinae and *T. geminatus* but absent in other species.
507 Geoisoptera-specific: Present in Termitidae and *R. grassei* but absent in other species.
508
509 Ancient: Present in Geoisoptera and either *C. secundus* or *Z. nevadensis*. Since *C. secundus* and
510 *Z. nevadensis* diverged from Geoisoptera between 120 to 140 million years ago, we classified
511 TE families in these two species within the same age group.
512
513 Note that our analysis of TE age did not explicitly address the effects of horizontal transfer,
514 which can make young TEs appear older once they enter different lineages. We defined TE age
515 based on phylogenetic distribution. Any TE family that violated the termite phylogeny (e.g.,
516 present only in *C. secundus* and *M. bellicosus* but absent in other species), and was therefore
517 likely derived from horizontal transfer, was categorized as "unknown age" and excluded from
518 our age-association analyses (e.g., TE age versus methylation level). Therefore, the impact of
519 horizontal transfer on our conclusions should be limited.
520
521 **Quantification of TE abundance**

522 TE abundance was quantified at the TE family and the TE superfamily level. For TE family
523 level abundance quantification, we used the copy numbers derived from the summarized output
524 of the One-code-to-find-them-all tool (see *Repeat annotation in genome assemblies*). For TE
525 superfamily level quantification, we used the sum of the copy numbers of all TE families that
526 have been classified under the same TE superfamily for each respective superfamily.
527
528 **Identification of structure variants with *M. bellicosus* population genomes**

529 The Sniffles2 pipeline (v2.4) [96] (default parameters) was used for structure variants (SVs)
530 identification. The PacBio reads of each *M. bellicosus* individual sample were mapped onto the
531 *M. bellicosus* queen genome assembly using Minimap (v2.28) [97] (default parameters for HiFi

532 reads). Population SVs were then identified with Sniffles multi-sample SV calling. For each
533 SV location (which can include multiple SVs from different individuals), the longest SV
534 sequence was extracted as the representative SV.
535
536 **Annotation and quantification of TE-associated SVs**

537 We employed RepeatMasker to annotate SV sequences, using our termite non-redundant repeat
538 library as the reference library. In addition, we also used *blastn* (with the *megablast* program)
539 (v2.16) [98] to annotate the SV sequences by blasting against the repeat library and retaining the
540 best-matched hits. We observed similar results for the annotated TE-associated SVs with both
541 methods but the RepeatMasker method can also identify simple repeats. We therefore used the
542 result from the RepeatMasker method for downstream analyses.
543
544 For the quantification of TE-associated SVs at the TE family level, we used the total number
545 of SV copies from the same TE family. For the quantification at the superfamily level, we
546 added the SV copies from all TE families that are classified under the same superfamily.
547
548 **Measurement of TE spreading efficiency**

549 Because TE families with high abundances in the genome are more likely to be associated with
550 SVs (Spearman's $r = 0.72$, $p < 1e\text{-}5$), we normalized the impact of TE abundance on the
551 number of SVs using TE spreading efficiency. TE spreading efficiency was calculated as the
552 total number of TE-associated SVs divided by the copy number of the target TE family within
553 the genome (*M. bellicosus*).
554
555 **Inferring the evolutionary history of TE families based on Kimura Distances (KDs)**

556 For each TE family in a genome, KDs were quantified for each TE copy by (1) aligning its
557 sequence to the consensus sequence of the corresponding TE family, and (2) calculating the
558 divergence using a modified Kimura 2-Parameter model, in which CG dinucleotide sites in the
559 consensus sequence were treated with special consideration [51]. Following the quantification of
560 the KDs, we inferred the evolutionary history of TE families by plotting their KD distribution
561 as histograms. Within each histogram, the presence of a single mode with a low median KD (<
562 10) indicates a recent expansion of the TE family. Conversely, a single mode with
563 a high median KD (> 20) indicates the presence of inactive TEs with ancient origins, often
564 referred to as TE remnants. Additionally, a mixture of both, characterized by
565 a bimodal distribution, implies a mixed evolutionary history.
566
567 **Identification of methylated DNA CpG sites**

568 PacBio HiFi reads contain kinetic information that reflects CpG 5-Methylcytosine (5mC)
569 modifications [99]. We thus used *Jasmine* (v. 2.0.0) (default parameters) to predict the CpG 5mC
570 for our HiFi read sequences. The HiFi reads with annotated 5mC information were then mapped
571 to the corresponding genome assembly with *minimap2 (pbmm2,* v. 1.12.0*)*. To filter suspicious
572 read alignments, we further used *samclip* to remove aligned reads with soft-clipped. With the
573 aligned reads, we calculated the CpG-site methylation probabilities for each genome assembly

using PacBio's *pb-CpG-tools* (*aligned_bam_to_cpg_scores* with the *model* pileup mode, v. 2.3.2), a machine-learning-based method for genomic CpG 5mC quantification.

For a robust determination of genomic CpG 5mC methylation, we only retained CpG sites with a read coverage between 10 to 50x, a CpG site was considered methylated when its CpG-site methylation probability was over 80%.

Quantification of TE methylation levels

To quantify the CpG methylation level in different genomic regions and different TE families, we first used the R package *GenomicRanges* [100] to determine the total number of CpG sites in target genomic sequences. The percentage of methylated CpGs was then calculated as the number of methylated CpG sites divided by the total number of CpG sites in the target sequence. For methylation quantification at the TE family level (i.e., TE methylation), the percentage of methylated CpGs was calculated by summarising all CpGs sites across all copies of the target TE family. To avoid quantification uncertainty due to a small number of CpG sites, only TE families with over 30 CpG sites from all TE copies were retained for downstream analyses. For methylation quantification at the TE superfamily level, the percentage of methylated CpGs was calculated as the median of the percentages of methylated CpGs across all associated families. Normalised TE methylation levels were then calculated as the ratio of the percentage of methylated CpGs in the target region or TE family/superfamily to the percentage of methylated CpGs in the genomic background. Therefore, a value > 1 indicates a higher percentage of CpG methylation relative to the genomic background, whereas a value < 1 signifies a lower percentage.

Principal component analyses (PCA) and clustering analyses on TE abundance and methylation levels

For PCA and clustering analyses of TE abundance across the termite genome assemblies, TE abundances were summarized at the superfamily level (see *Quantification of TE abundance*). The superfamily level TE abundances were $\log_{10}$ transformed (with one added pseudo-count to avoid $\log_{10} 0$). For PCA and clustering analyses of TE methylation levels across the termite genome assemblies, TE methylation levels were summarized at the superfamily level (see *Quantification of CpG methylation levels in TEs*) and standardized within each genome assembly. The standardization within a genome assembly is necessary because the sequencing depth differences across genome assemblies can influence the confidence of modelling CpG methylation probability.

The transformed TE abundance and the standardized TE methylation levels were then analysed with the R package *FactoMineR* [101] and clustered with the R package *pheatmap* [102].

Modelling the relationship between TEs and DNA methylation

The statistical relationship among TE family abundance, TE CpG methylation levels and TE age was tested using analysis of covariance (ANCOVA) in R [103] with the model:

log10(TE abundance + 1) ~ TE methylation X *TE age.*

The statistical relationship among TE family spreading efficiency, TE methylation levels and TE age was tested using ANCOVA with the model:

log10(TE spreading efficiency + *1) ~ TE methylation x TE age.*

To examine the effect size of DNA methylation on TE spreading efficiency across different TE age groups, a Spearman's correlation test was performed to assess the relationship between TE methylation levels and TE spreading efficiency for each age group.

Annotation of TE defence genes and homologous genes

We first searched FlyBase [104] and previous publications [31] to compile a set of TE defence-related genes, including those associated with DNA methylation, retrotransposon silencing, and piRNA processing. Next, we identified representative homologs of these TE defence genes in published termite/cockroach genomes with NCBI Orthologs [105]. For a TE defence gene with multiple homologs in the same species (e.g., due to gene duplication), we retained all homologs and appended *_N* suffix to their names. For a TE defence gene with multiple single orthologs across different species, we retained the longest-matched ortholog as the representative.

We then collected the protein sequences of these representative TE defence gene orthologs as reference and aligned them to our termite and the woodroach genome assemblies with Miniprot (v0.13) [106]. For each target genome, we retained the best-matched Miniprot hits as the TE defence gene homologs.

For whole genome homolog annotation, we followed a similar procedure but used the protein sequences (longest protein isoforms) from *M. bellicosus* as the reference for Miniprot.

Detection of positive selection in TE defence genes

To detect positive selection, we first aligned the orthologous coding nucleotide sequences from the termite and the woodroach genome assemblies. The alignment was done using the MACSE pipeline (v12.01) (default parameters), which employs codon-aware alignment and filters out non-homologous and misaligned fragments and sequences [107]. We then used HyPhy (Hypothesis testing using phylogenies) (v2.5.62) [108] to perform the branch-site unrestricted statistical test for episodic diversification (BUSTED) model [53] and the adaptive branch-site random effects likelihood (aBSREL) model [54]. The BUSTED model detected whether a target gene has experienced overall positive selection, while the aBSREL model identified the lineages or species in which the gene has undergone positive selection. To reduce false positive, false discovery rate (FDR) was applied on the p-values for multiple test correction.

Data availability

PacBio HiFi-reads for the termite genome assemblies have been deposited under Bioproject accession number PRJNA1033592 (https://dataview.ncbi.nlm.nih.gov/object/PRJNA1033592?reviewer=14aemg42gu201rtpms2o2e1huh).

Code availability

The shell and R scripts used to process the data are available on https://github.com/BitaoQiu/termites_TE_methylation.

Acknowledgements

We thank Franck Dedeine for providing the *Reticulitermes grassei* lab colony for genome sequencing, Kiyoto Maekawa for access to the *Cryptocercus punctulatus* genome before it was published, and Daniela Schnaiter for carefully looking after the termite colonies. We acknowledge the support of the Baden-Württemberg High-Performance Computing facilities and the Deutsche Forschungsgemeinschaft (DFG) through grant INST 35/1597-1 FUGG. Charles Darwin University (Australia), and especially S. Garnett and the Horticulture and Aquaculture team, provided logistic support to collect *Cryptotermes secundus* and *Mastotermes darwiniensis*. The Parks and Wildlife Commission, Northern Territory, the Department of the Environment, Water, Heritage and the Arts gave permission to collect (permit number 64452 & 71896) and export (permit PWS2019-AU-000897) the termites. We thank B. Sinsin for providing collection permits for Benin, N. Kone for logistic support in Côte d'Ivoire and the Office Ivoirien des Parcs et Réserves provided sampling and export permits for samples from Côte d'Ivoire. The study was conducted in accordance with the Nagoya protocol. This work was supported by the DFG Research Infrastructure West German Genome Center, project 407493903, as part of the Next Generation Sequencing Competence Network, project 423957469. Next Generation Sequencing was carried out at the West German Genome Center Düsseldorf. BQ was supported by a Humboldt Research Fellowship for Postdoctoral Researchers from the Alexander von Humboldt Foundation. In addition, this research was supported by the DFG with two grants to JK, one within the 'Sequencing cost in projects #1' initiative (DFG; KO1895/26-1, 29-1).

Author contributions

B.Q. and J.K. designed the project and experiments. B.Q., D.E., J.K. collected samples. B.Q. and D.E. performed the experiment and collected the data. B.Q. did the analyses. B.Q. and J.K. wrote the first draft of the manuscript. All authors contributed to the interpretation of experimental results and final manuscript revisions.

Competing interests

The authors declare no competing interests.

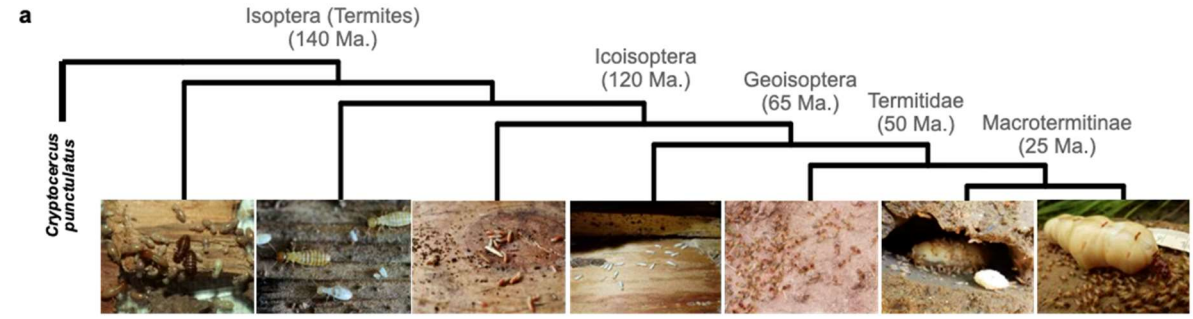

	Mastotermes darwiniensis	*Zootermppsis nevadensis*	*Cryptotermes secundus*	*Reticulitermes grassei*	*Trinervitermes geminatus*	*Odontotermes* sp.2	*Macrotermes bellicosus*
Genome size	1.35 Gb	0.58 Gb	1.30 Gb	1.00 Gb	1.45 Gb	1.47 Gb	1.34 Gb
Repeat size (%)	0.82 Gb (61.3%)	0.23 Gb (40.5 %)	0.79 Gb (60.5%)	0.49 Gb (49.4%)	0.83 Gb (56.9%)	0.88 Gb (59.9%)	0.75 Gb (55.8%)
% CpG met.	3 %	8 %	8 %	7 %	9 %	3 %	8 %
BUSCO coverage	99.8 %	100 %	99.8 %	99.8 %	98.8 %	99.8 %	99.9 %

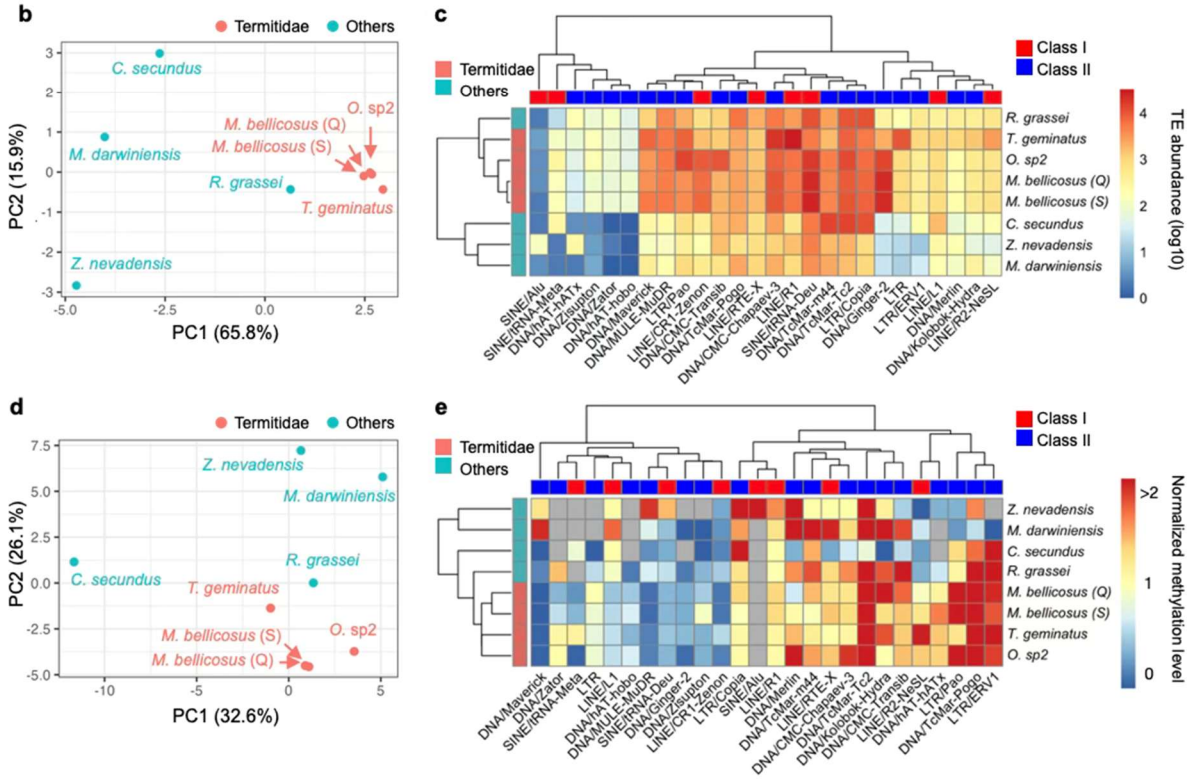

Figure 1. TEs and TE methylation patterns have strong evolutionary signals in termites.

a Cladogram and overall genome statistics (genome size, repeat contents, genome wide methylation level and BUSCO gene content completeness) of the seven studied termite species. The phylogenetic tree of termites is based on [45,46]. **b** PCA of TE superfamily abundances ($n = 71$) in the termite genomes, coloured according to species taxonomy. **c** Heatmap of TE superfamily abundances for the top 26 TE superfamilies showing the highest variation in abundance or CpG methylation across species. Abundances are shown on a $\log_{10}$ scale. **d** PCA of TE superfamily CpG methylation levels ($n = 69$) in the termite genomes, coloured according to termite taxonomy. **e** Heatmap of normalized CpG methylation levels for the same TE superfamilies as in panel **c**. Normalised methylation levels range from 0 (devoid of methylated CpG sites), 1 (equal to the genomic background), to > 2 (over two folds higher than the genomic background). The normalised methylation level was calculated as the ratio of

711 the percentage of methylated CpG sites in a TE superfamily to that in the genome. TE superfamilies
712 are coloured in grey when methylation information were unavailable due low abundance, For *M.*
713 *bellicosu*s, both a queen (Q) and a soldier (S) genome were included.

714

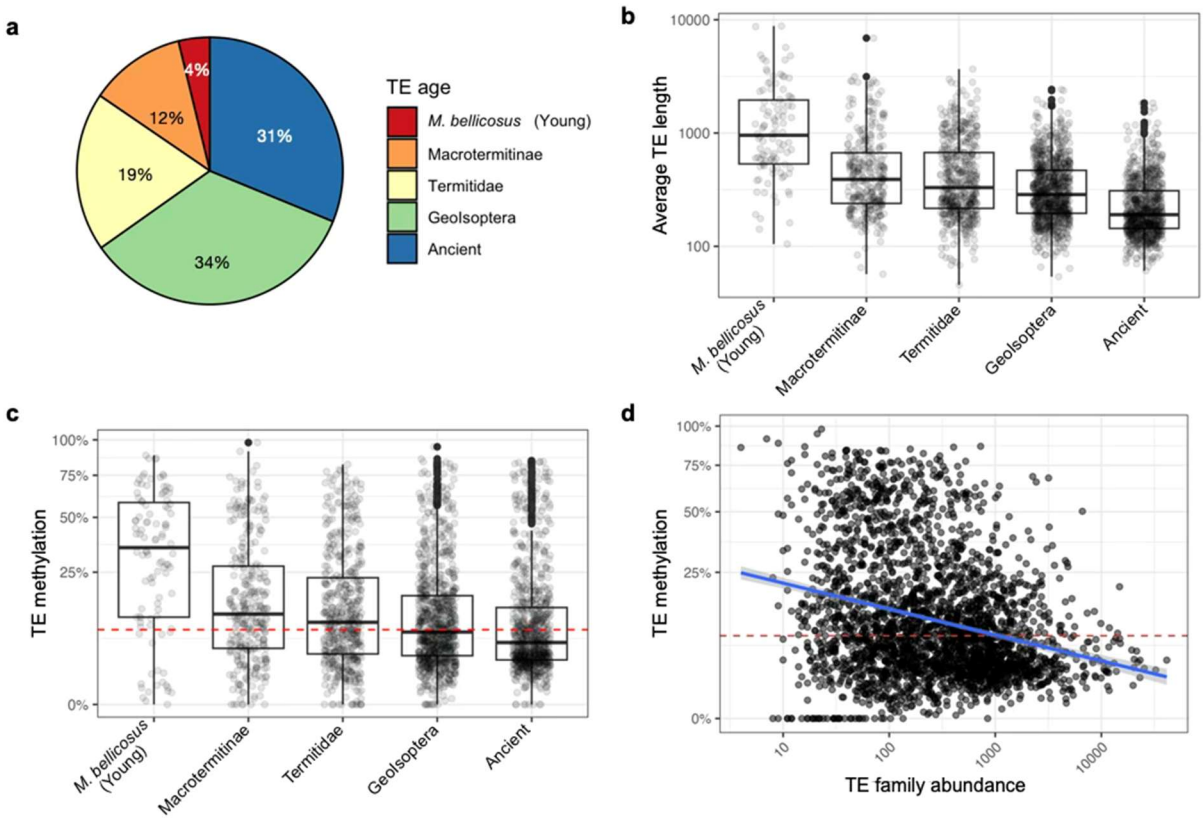

Figure 2. Age dynamics of TE families and TE methylation in *M. bellicosus*

a Pie-chart of the age distribution of TE families (n = 2672) in *M. bellicosus*. TE family ages were estimated based on the distribution of TE families across the termite phylogeny. 'Ancient' means TE families older than the last common ancestor of Neoisoptera and *C. secundus*. **b** Boxplots of average sequence length for TE families from different TE age groups. The average sequence length was calculated as the total sequence length of a TE family divided by its copy number. **c** Boxplots of the percentages of methylated CpG sites for TE families from different TE age groups. **d** The association between the percentage of TE methylation and TE family abundance. We found a similar pattern in other termite genomes (**Supplementary Fig. 3**). For **b**, **c** and **d**, each point represents one TE family. The red dashed lines in **c** and **d** represent the background genomic methylation level (8%) of *M. bellicosus*.

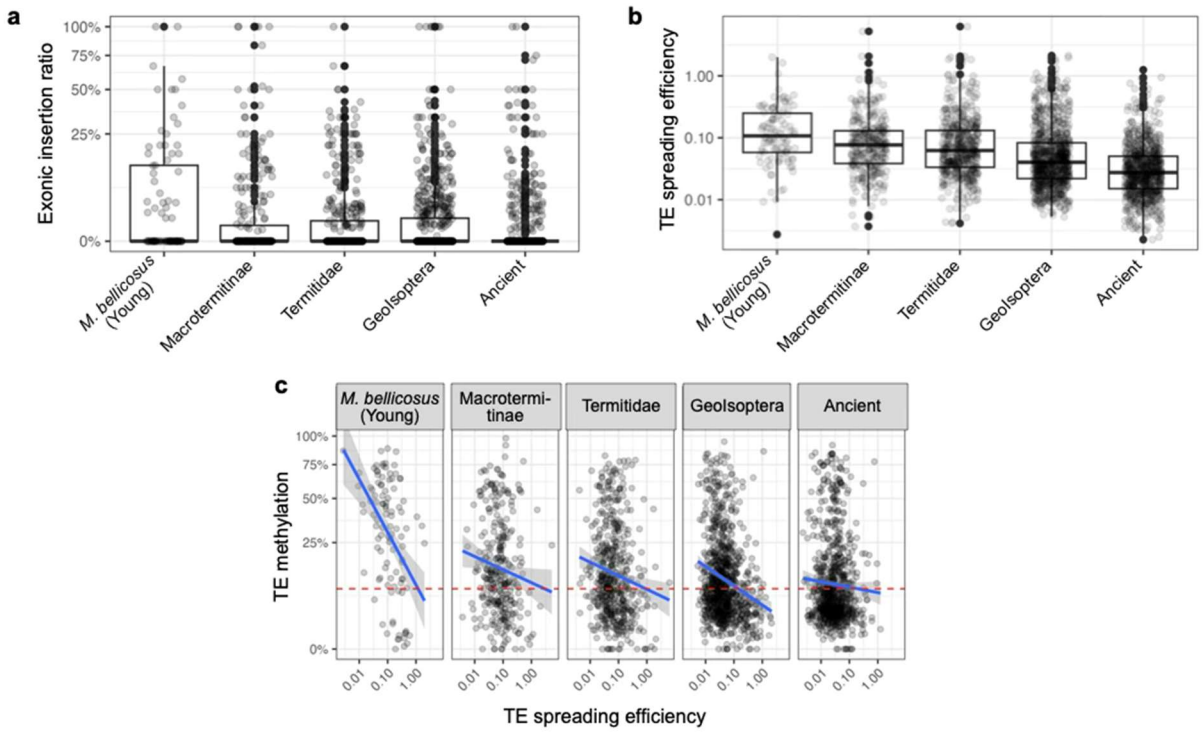

Figure 3. TE activity reveals TE and TE methylation arms race dynamics in *M. bellicosus*

a Boxplots of exonic insertion ratios of TE-associated SVs (structural variants) across different TE ages. The exonic insertion ratio was calculated as the percentage of exonic insertions to the total number of insertions per family. **b** Boxplots of the TE spreading efficiency across different TE ages. **c** The association between TE spreading efficiencies and TE methylation levels, plotted separately for each TE age group. Blue lines represent regression lines. The red dashed line represents the background genomic methylation level (8%) of *M. bellicosus*. For **a**, **b**, and **c**, each point represents one TE family. For **b** and **c**, TE spreading efficiency was calculated as the number of TE-associated SVs normalised by TE family abundance.

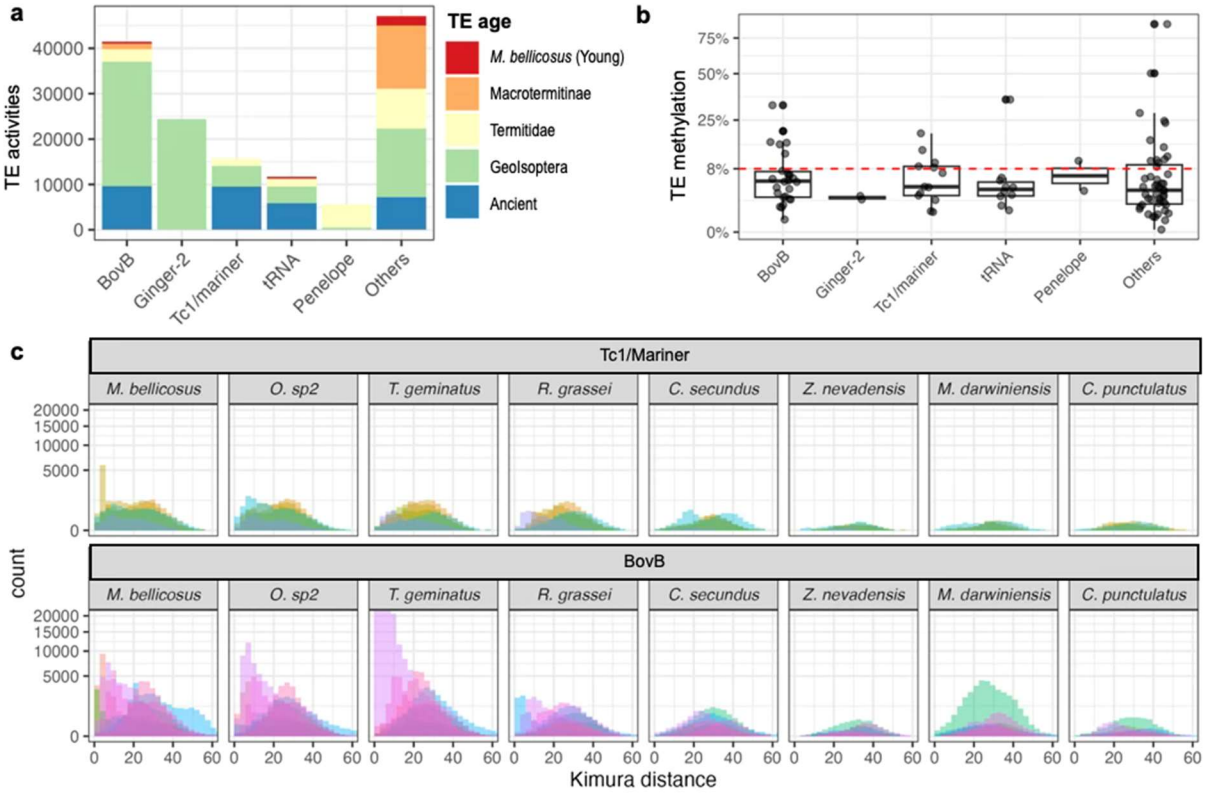

Figure 4. Top active TE families can have ancient origins

a Activity levels of the top 100 active TE families in *M. bellicosus*. TE families are grouped by superfamilies and coloured by TE age, ranging from young, *M. bellicosus*-specific (red) to ancient (blue) TE families. TE activity levels are quantified by the copy number of TE-associated SVs in a *M. bellicosus* population ($N = 6$ genomes). The top five active TE superfamilies are shown separately; the remaining are grouped as Others. **b** The percentages of methylated CpG sites for the top 100 active TE families, grouped by superfamilies. Only the top 5 most active TE superfamilies are shown. The red dotted line represents the genomic methylation level (8%) of *M. bellicosus*. **c** Histograms of Kimura distances (KD) for the top active Tc1/Mariner (upper panel, $n = 5$) and BovB (lower panel, $n = 8$) ancient TE families, plotted separately for each species. Each colour represents one TE family. A low KD value indicates recent TE expansion/invasion and a high KD value suggests TE remnants that have been inactive for a long time.

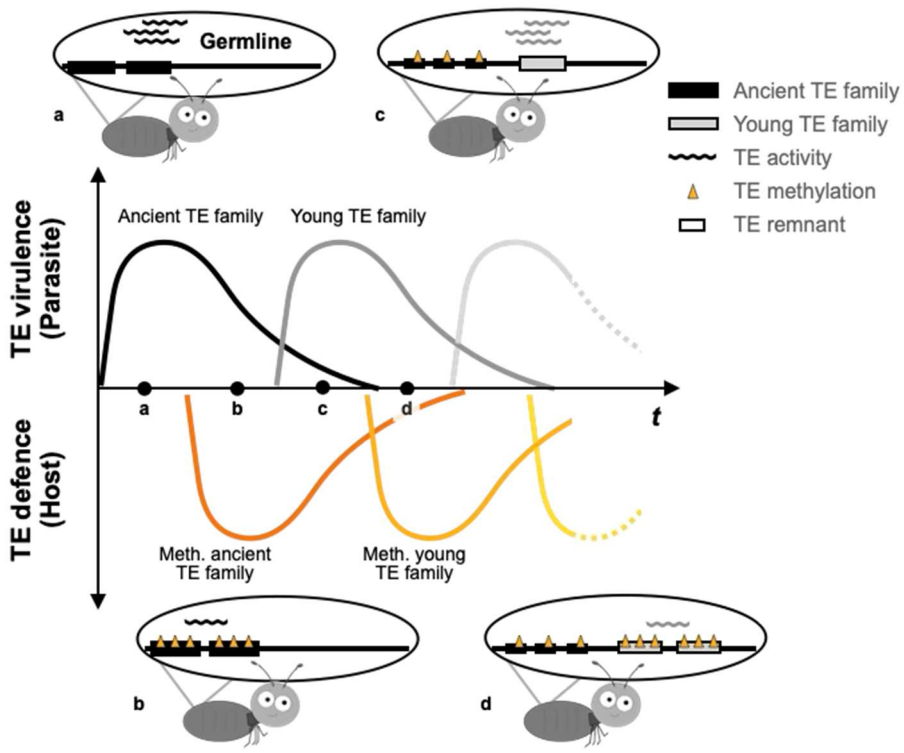

Figure 5. A schematic diagram of the arms race between TEs and TE defence

a TEs can behave as genomic parasites, whose unchecked proliferation can cause significant harm to their hosts. **b** In response, natural selection favours hosts that evolve molecular defence systems, such as DNA methylation, to suppress these genomic parasites and limit their spread. **c** Over evolutionary time, once-rampant ancient TE families gradually lose their virulence, by reduced spreading efficiency, fewer exonic insertions, and degeneration into TE remnants. As their threat wanes, so does the selective pressure on the host to maintain costly defences, leading to reduced TE methylation. Yet young TE families emerge, launching fresh invasions into the host genome. **d** This ever-renewing arms race selects hosts to once again ramp up their defences, reinforcing methylation-based suppression against new TE families. At the same time, some TEs can be co-opted by the host, causing evolutionary innovations and shifting the relationship from parasitism to mutualism (not shown).

767 **References**

768

769 1. Dawkins, R. & Krebs, J. R. Arms races between and within species. *Proc. R. Soc. Lond.*
770 *Ser. B Biol. Sci.* **205**, 489–511 (1979).

771 2. Goerlitz, H. R., Hofstede, H. M. ter, Zeale, M. R. K., Jones, G. & Holderied, M. W. An
772 aerial-hawking bat uses stealth echolocation to counter moth hearing. *Curr. Biol.* **20**, 1568–
773 1572 (2010).

774 3. Fullard, J. H., Ratcliffe, J. M. & Soutar, A. R. Extinction of the acoustic startle response in
775 moths endemic to a bat-free habitat. *J. Evol. Biol.* **17**, 856–861 (2004).

776 4. Ågren, J. A. Evolutionary transitions in individuality: insights from transposable elements.
777 *Trends Ecol. Evol.* **29**, 90–96 (2014).

778 5. Cosby, R. L., Chang, N.-C. & Feschotte, C. Host–transposon interactions: conflict,
779 cooperation, and cooption. *Genes Dev.* **33**, 1098–1116 (2019).

780 6. Lawlor, M. A. & Ellison, C. E. Evolutionary dynamics between transposable elements and
781 their host genomes: mechanisms of suppression and escape. *Curr. Opin. Genet. Dev.* **82**,
782 102092 (2023).

783 7. Luo, S. *et al.* The evolutionary arms race between transposable elements and piRNAs in
784 Drosophila melanogaster. *BMC Evol. Biol.* **20**, 14 (2020).

785 8. Wells, J. N. & Feschotte, C. A field guide to eukaryotic transposable elements. *Annu. Rev.*
786 *Genet.* **54**, 1–23 (2020).

787 9. Wicker, T. *et al.* A unified classification system for eukaryotic transposable elements. *Nat.*
788 *Rev. Genet.* **8**, 973–982 (2007).

789 10. Volff, J. Turning junk into gold: domestication of transposable elements and the creation
790 of new genes in eukaryotes. *BioEssays* **28**, 913–922 (2006).

791 11. Biémont, C. A brief history of the status of transposable elements: from junk DNA to
792 major players in evolution. *Genetics* **186**, 1085–1093 (2010).

793 12. González, J. & Petrov, D. A. The adaptive role of transposable elements in the Drosophila
794 genome. *Gene* **448**, 124–133 (2009).

795 13. Oomen, M. E. *et al.* An atlas of transcription initiation reveals regulatory principles of
796 gene and transposable element expression in early mammalian development. *Cell* **188**, 1156-
797 1174.e20 (2025).

798 14. Kidwell, M. G. & Lisch, D. R. Perspective: transposable elements, parasitic DNA, and
799 genome evolution. *Evolution* **55**, 1–24 (2001).

800 15. Barrón, M. G., Fiston-Lavier, A.-S., Petrov, D. A. & González, J. Population genomics of
801 transposable elements in Drosophila. *Annu. Rev. Genet.* **48**, 1–21 (2014).

802 16. Bourque, G. *et al.* Ten things you should know about transposable elements. *Genome*
803 *Biol.* **19**, 199 (2018).

804 17. Robillard, É., Rouzic, A. L., Zhang, Z., Capy, P. & Hua-Van, A. Experimental evolution
805 reveals hyperparasitic interactions among transposable elements. *Proc. Natl. Acad. Sci.* **113**,
806 14763–14768 (2016).

807 18. Czech, B. & Hannon, G. J. One loop to rule them all: the ping-pong cycle and piRNA-
808 guided silencing. *Trends Biochem. Sci.* **41**, 324–337 (2016).

809 19. Siomi, M. C., Sato, K., Pezic, D. & Aravin, A. A. PIWI-interacting small RNAs: the
810 vanguard of genome defence. *Nat. Rev. Mol. Cell Biol.* **12**, 246–258 (2011).

811 20. Betancourt, A. J., Wei, K. H.-C., Huang, Y. & Lee, Y. C. G. Causes and consequences of
812 varying transposable element activity: an evolutionary perspective. *Annu. Rev. Genom. Hum.*
813 *Genet.* **25**, 1–25 (2024).

814 21. Ågren, J. A., Davies, N. G. & Foster, K. R. Enforcement is central to the evolution of
815 cooperation. *Nat Ecol Evol* **3**, 1018–1029 (2019).

816 22. Pritam, S. & Signor, S. Evolution of piRNA-guided defense against transposable
817 elements. *Trends Genet.* (2024) doi:10.1016/j.tig.2024.11.011.

818 23. Ying, H. *et al.* The role of DNA methylation in genome defense in Cnidaria and other
819 invertebrates. *Mol. Biol. Evol.* **39**, msac018- (2022).

820 24. Zhang, H., Lang, Z. & Zhu, J.-K. Dynamics and function of DNA methylation in plants.
821 *Nat. Rev. Mol. Cell Biol.* **19**, 489–506 (2018).

822 25. Zhou, W., Liang, G., Molloy, P. L. & Jones, P. A. DNA methylation enables transposable
823 element-driven genome expansion. *Proc. Natl. Acad. Sci.* **117**, 19359–19366 (2020).

824 26. Wang, X., Ramat, A., Simonelig, M. & Liu, M.-F. Emerging roles and functional
825 mechanisms of PIWI-interacting RNAs. *Nat. Rev. Mol. Cell Biol.* **24**, 123–141 (2023).

826 27. Iwasaki, Y. W., Shoji, K., Nakagwa, S., Miyoshi, T. & Tomari, Y. Transposon–host arms
827 race: a saga of genome evolution. *Trends Genet.* **41**, 369–389 (2025).

828 28. Delanoue, R., Clot, C., Leray, C., Pihl, T. & Hudry, B. Y chromosome toxicity does not
829 contribute to sex-specific differences in longevity. *Nat. Ecol. Evol.* **7**, 1245–1256 (2023).

830 29. Sturm, Á., Ivics, Z. & Vellai, T. The mechanism of ageing: primary role of transposable
831 elements in genome disintegration. *Cell. Mol. Life Sci.* **72**, 1839–1847 (2015).

832 30. Wood, J. G. *et al.* Chromatin-modifying genetic interventions suppress age-associated
833 transposable element activation and extend life span in Drosophila. *Proc. Natl. Acad. Sci.* **113**,
834 11277–11282 (2016).

835 31. Elsner, D., Meusemann, K. & Korb, J. Longevity and transposon defense, the case of
836 termite reproductives. *Proc National Acad Sci* **115**, 5504–5509 (2018).

32. Gorbunova, V. *et al.* The role of retrotransposable elements in ageing and age-associated diseases. *Nature* **596**, 43–53 (2021).

33. Korb, J. *et al.* A genomic comparison of two termites with different social complexity. *Front. Genet.* **6**, 9 (2015).

34. Harrison, M. C. *et al.* Hemimetabolous genomes reveal molecular basis of termite eusociality. *Nat. Ecol. Evol.* **2**, 557–566 (2018).

35. Kuhn, J. M. M., Meusemann, K. & Korb, J. Disentangling the aging gene expression network of termite queens. *BMC Genom.* **22**, 339 (2021).

36. Petersen, M. *et al.* Diversity and evolution of the transposable element repertoire in arthropods with particular reference to insects. *BMC Ecol. Evol.* **19**, 11 (2019).

37. Glastad, K. M., Gokhale, K., Liebig, J. & Goodisman, M. A. D. The caste- and sex-specific DNA methylome of the termite Zootermopsis nevadensis. *Sci. Rep.* **6**, 37110 (2016).

38. Harrison, M. C. *et al.* Complex regulatory role of DNA methylation in caste- and age-specific expression of a termite. *Open Biol.* **12**, 220047 (2022).

39. Krueger, F., Kreck, B., Franke, A. & Andrews, S. R. DNA methylome analysis using short bisulfite sequencing data. *Nat. Methods* **9**, 145–151 (2012).

40. Ni, P. *et al.* DNA 5-methylcytosine detection and methylation phasing using PacBio circular consensus sequencing. *Nat. Commun.* **14**, 4054 (2023).

41. Ahsan, M. U., Gouru, A., Chan, J., Zhou, W. & Wang, K. A signal processing and deep learning framework for methylation detection using Oxford Nanopore sequencing. *Nat. Commun.* **15**, 1448 (2024).

42. Hanada, T. *et al.* Differential expression of hormone-related genes in the heads of adult and nymphal woodroaches (Cryptocercus). *J. Exp. Zoöl. Part B: Mol. Dev. Evol.* (2025) doi:10.1002/jez.b.23290.

43. Suh, A. Genome size evolution: small transposons with large consequences. *Curr. Biol.* **29**, R241–R243 (2019).

44. Chak, S. T. C., Harris, S. E., Hultgren, K. M., Jeffery, N. W. & Rubenstein, D. R. Eusociality in snapping shrimps is associated with larger genomes and an accumulation of transposable elements. *Proc. Natl. Acad. Sci.* **118**, e2025051118 (2021).

45. Bucek, A. *et al.* Evolution of termite symbiosis informed by transcriptome-based phylogenies. *Curr Biol* **29**, 3728-3734.e4 (2019).

46. Hellemans, S. *et al.* Genomic data provide insights into the classification of extant termites. *Nat. Commun.* **15**, 6724 (2024).

47. Rouzic, A. L., Boutin, T. S. & Capy, P. Long-term evolution of transposable elements. *Proc. Natl. Acad. Sci.* **104**, 19375–19380 (2007).

872 48. Kofler, R., Senti, K.-A., Nolte, V., Tobler, R. & Schlötterer, C. Molecular dissection of a
873 natural transposable element invasion. *Genome Res.* **28**, 824–835 (2018).

874 49. Carelli, F. N. *et al.* Widespread transposon co-option in the Caenorhabditis germline
875 regulatory network. *Sci. Adv.* **8**, eabo4082 (2022).

876 50. Chalopin, D., Naville, M., Plard, F., Galiana, D. & Volff, J.-N. Comparative analysis of
877 transposable elements highlights mobilome diversity and evolution in vertebrates. *Genome*
878 *Biol. Evol.* **7**, 567–580 (2015).

879 51. Kimura, M. A simple method for estimating evolutionary rates of base substitutions
880 through comparative studies of nucleotide sequences. *J. Mol. Evol.* **16**, 111–120 (1980).

881 52. Brouha, B. *et al.* Hot L1s account for the bulk of retrotransposition in the human
882 population. *Proc. Natl. Acad. Sci.* **100**, 5280–5285 (2003).

883 53. Murrell, B. *et al.* Gene-wide identification of episodic selection. *Mol. Biol. Evol.* **32**,
884 1365–1371 (2015).

885 54. Smith, M. D. *et al.* Less is more: an adaptive branch-site random effects model for
886 efficient detection of episodic diversifying selection. *Mol. Biol. Evol.* **32**, 1342–1353 (2015).

887 55. Van, V. A new evolutionary law. *Evolutionary theory* **1**, 1 (1973).

888 56. Werren, J. H. Selfish genetic elements, genetic conflict, and evolutionary innovation.
889 *Proc. Natl. Acad. Sci.* **108**, 10863–10870 (2011).

890 57. Post, F., Bornberg-Bauer, E., Vasseur-Cognet, M. & Harrison, M. C. More effective
891 transposon regulation in fertile, long-lived termite queens than in sterile workers. *Mol. Ecol.*
892 **32**, 369–380 (2023).

893 58. Bewick, A. J., Vogel, K. J., Moore, A. J. & Schmitz, R. J. Evolution of DNA methylation
894 across insects. *Mol. Biol. Evol.* **34**, 654–665 (2017).

895 59. Provataris, P., Meusemann, K., Niehuis, O., Grath, S. & Misof, B. Signatures of DNA
896 methylation across insects suggest reduced DNA methylation levels in Holometabola.
897 *Genome Biol. Evol.* **10**, evy066- (2018).

898 60. Lewis, S. H. *et al.* Widespread conservation and lineage-specific diversification of
899 genome-wide DNA methylation patterns across arthropods. *PLoS Genet.* **16**, e1008864
900 (2020).

901 61. Snyman, M. & Xu, S. The effects of mutations on gene expression and alternative
902 splicing. *Proc. R. Soc. B* **290**, 20230565 (2023).

903 62. Lockton, S., Ross-Ibarra, J. & Gaut, B. S. Demography and weak selection drive patterns
904 of transposable element diversity in natural populations of Arabidopsis lyrata. *Proc. Natl.*
905 *Acad. Sci.* **105**, 13965–13970 (2008).

906 63. Lynch, M. *The Origins of Genome Architecture*. (Sunderland (Mass.) : Sinauer associates,
907 2007).

908 64. Ellison, C. E., Kagda, M. S. & Cao, W. Telomeric TART elements target the piRNA
909 machinery in Drosophila. *PLoS Biol.* **18**, e3000689 (2020).

910 65. Zhang, H.-H., Peccoud, J., Xu, M.-R.-X., Zhang, X.-G. & Gilbert, C. Horizontal transfer
911 and evolution of transposable elements in vertebrates. *Nat. Commun.* **11**, 1362 (2020).

912 66. Peccoud, J., Loiseau, V., Cordaux, R. & Gilbert, C. Massive horizontal transfer of
913 transposable elements in insects. *Proc. Natl. Acad. Sci.* **114**, 4721–4726 (2017).

914 67. Senft, A. D. & Macfarlan, T. S. Transposable elements shape the evolution of mammalian
915 development. *Nat. Rev. Genet.* **22**, 691–711 (2021).

916 68. Schmidleithner, L., Stüve, P. & Feuerer, M. Transposable elements as instructors of the
917 immune system. *Nat. Rev. Immunol.* **25**, 696–706 (2025).

918 69. Chuong, E. B., Elde, N. C. & Feschotte, C. Regulatory activities of transposable elements:
919 from conflicts to benefits. *Nat. Rev. Genet.* **18**, 71–86 (2017).

920 70. Arribas, Y. A. *et al.* Transposable element exonization generates a reservoir of evolving
921 and functional protein isoforms. *Cell* **187**, 7603-7620.e22 (2024).

922 71. Schrader, L. & Schmitz, J. The impact of transposable elements in adaptive evolution.
923 *Mol. Ecol.* **28**, 1537–1549 (2019).

924 72. Jangam, D., Feschotte, C. & Betrán, E. Transposable Element Domestication As an
925 Adaptation to Evolutionary Conflicts. *Trends Genet.* **33**, 817–831 (2017).

926 73. Fuchs, A., Heinze, J., Reber-Funk, C. & Korb, J. Isolation and characterization of six
927 microsatellite loci in the drywood termite Cryptotermes secundus (Kalotermitidae). *Mol. Ecol.*
928 *Notes* **3**, 355–357 (2003).

929 74. Cheng, H., Concepcion, G. T., Feng, X., Zhang, H. & Li, H. Haplotype-resolved de novo
930 assembly using phased assembly graphs with hifiasm. *Nat. Methods* **18**, 170–175 (2021).

931 75. Ko, B. J. *et al.* Widespread false gene gains caused by duplication errors in genome
932 assemblies. *Genome Biol.* **23**, 205 (2022).

933 76. Guan, D. *et al.* Identifying and removing haplotypic duplication in primary genome
934 assemblies. *Bioinformatics* **36**, 2896–2898 (2020).

935 77. Astashyn, A. *et al.* Rapid and sensitive detection of genome contamination at scale with
936 FCS-GX. *Genome Biol.* **25**, 60 (2024).

937 78. Manni, M., Berkeley, M. R., Seppey, M., Simão, F. A. & Zdobnov, E. M. BUSCO
938 Update: Novel and Streamlined Workflows along with Broader and Deeper Phylogenetic
939 Coverage for Scoring of Eukaryotic, Prokaryotic, and Viral Genomes. *Mol. Biol. Evol.* **38**,
940 4647–4654 (2021).

941 79. Rhie, A., Walenz, B. P., Koren, S. & Phillippy, A. M. Merqury: reference-free quality,
942 completeness, and phasing assessment for genome assemblies. *Genome Biol.* **21**, 245 (2020).

80. Ranallo-Benavidez, T. R., Jaron, K. S. & Schatz, M. C. GenomeScope 2.0 and Smudgeplot for reference-free profiling of polyploid genomes. *Nat. Commun.* **11**, 1432 (2020).

81. Flynn, J. M. *et al.* RepeatModeler2 for automated genomic discovery of transposable element families. *Proc. Natl. Acad. Sci.* **117**, 9451–9457 (2020).

82. Orozco-Arias, S., Sierra, P., Durbin, R. & González, J. MCHelper automatically curates transposable element libraries across eukaryotic species. *Genome Res.* **34**, 2256–2268 (2024).

83. Flutre, T., Duprat, E., Feuillet, C. & Quesneville, H. Considering Transposable Element Diversification in De Novo Annotation Approaches. *PLoS ONE* **6**, e16526 (2011).

84. Bao, W., Kojima, K. K. & Kohany, O. Repbase Update, a database of repetitive elements in eukaryotic genomes. *Mob. DNA* **6**, 11 (2015).

85. Storer, J., Hubley, R., Rosen, J., Wheeler, T. J. & Smit, A. F. The Dfam community resource of transposable element families, sequence models, and genome annotations. *Mob. DNA* **12**, 2 (2020).

86. Smit, A., Hubley, R. & P., G. *RepeatMasker Open-4.0.*

87. Bailly-Bechet, M., Haudry, A. & Lerat, E. "One code to find them all": a perl tool to conveniently parse RepeatMasker output files. *Mob. DNA* **5**, 13 (2014).

88. Gabriel, L. *et al.* BRAKER3: Fully automated genome annotation using RNA-seq and protein evidence with GeneMark-ETP, AUGUSTUS, and TSEBRA. *Genome Res.* **34**, 769–777 (2024).

89. Pertea, M., Kim, D., Pertea, G. M., Leek, J. T. & Salzberg, S. L. Transcript-level expression analysis of RNA-seq experiments with HISAT, StringTie and Ballgown. *Nat Protoc* **11**, 1650–1667 (2016).

90. Lin, S., Werle, J. & Korb, J. Transcriptomic analyses of the termite, Cryptotermes secundus, reveal a gene network underlying a long lifespan and high fecundity. *Commun Biology* **4**, 384 (2021).

91. Korb, J. *et al.* Comparative transcriptomic analysis of the mechanisms underpinning ageing and fecundity in social insects. *Philosophical Transactions Royal Soc B* **376**, 20190728 (2021).

92. Kim, D., Paggi, J. M., Park, C., Bennett, C. & Salzberg, S. L. Graph-based genome alignment and genotyping with HISAT2 and HISAT-genotype. *Nat. Biotechnol.* **37**, 907–915 (2019).

93. Tegenfeldt, F. *et al.* OrthoDB and BUSCO update: annotation of orthologs with wider sampling of genomes. *Nucleic Acids Res.* **53**, D516–D522 (2024).

94. BJ., H. *TransDecoder*.

95. Blum, M. *et al.* The InterPro protein families and domains database: 20 years on. *Nucleic Acids Res* **49**, D344–D354 (2020).

96. Smolka, M. *et al.* Detection of mosaic and population-level structural variants with Sniffles2. *Nat. Biotechnol.* **42**, 1571–1580 (2024).

97. Li, H. New strategies to improve minimap2 alignment accuracy. *Bioinformatics* **37**, 4572–4574 (2021).

98. Altschul, S. F., Gish, W., Miller, W., Myers, E. W. & Lipman, D. J. Basic local alignment search tool. *J Mol Biol* **215**, 403–410 (1990).

99. Flusberg, B. A. *et al.* Direct detection of DNA methylation during single-molecule, real-time sequencing. *Nat. Methods* **7**, 461–465 (2010).

100. Lawrence, M. *et al.* Software for computing and annotating genomic ranges. *PLoS Comput. Biol.* **9**, e1003118 (2013).

101. Lê, S., Josse, J. & Husson, F. FactoMineR: an R package for multivariate analysis. *J. Stat. Softw.* **25**, (2008).

102. Kolde, R. *Pretty Heatmaps*. (2022).

103. RCoreTeam. *R: A Language and Environment for Statistical Computing.* (2024).

104. Öztürk-Çolak, A. *et al.* FlyBase: updates to the Drosophila genes and genomes database. *GENETICS* **227**, iyad211 (2024).

105. Sayers, E. W. *et al.* Database resources of the National Center for Biotechnology Information. *Nucleic Acids Res.* **48**, D9–D16 (2019).

106. Li, H. Protein-to-genome alignment with miniprot. *Bioinformatics* **39**, btad014 (2023).

107. Ranwez, V., Douzery, E. J. P., Cambon, C., Chantret, N. & Delsuc, F. MACSE v2: toolkit for the alignment of coding sequences accounting for frameshifts and stop codons. *Mol. Biol. Evol.* **35**, 2582–2584 (2018).

108. Pond, S. L. K., Frost, S. D. W. & Muse, S. V. HyPhy: hypothesis testing using phylogenies. *Bioinformatics* **21**, 676–679 (2004).